NRC Publications Archive
Archives des publications du CNRC

In situ measurement and modelling of austenite grain growth in a Ti/Nb microalloyed steel
Maalekian, M.; Radis, R.; Militzer, M.; Moreau, A.; Poole, W. J.

NRC Publications Record / Notice d'Archives des publications de CNRC:
https://nrc-publications.canada.ca/eng/view/object/?id=457813a2-ac40-466c-9633-c16ed3dc49e8
https://publications-cnrc.canada.ca/fra/voir/objet/?id=457813a2-ac40-466c-9633-c16ed3dc49e8

National Research Council Canada   Conseil national de recherches Canada

Canada

In situ measurement and modelling of austenite grain growth in a Ti/Nb microalloyed steel

M. Maalekian [a,*], R. Radis [b,c], M. Militzer [a], A. Moreau [d], W.J. Poole [a]

[a] The Centre for Metallurgical Process Engineering, The University of British Columbia, Vancouver, BC, Canada V6T 1Z4
[b] Christian Doppler Laboratory "Early Stages of Precipitation", Institute of Materials Science and Technology,
Vienna University of Technology, Favoritenstraße 9-11, 1040 Vienna, Austria
[c] Institute for Materials Science and Welding, Graz University of Technology, Kopernikusgasse 24, Graz 8010, Austria
[d] Industrial Materials Institute, National Research Council of Canada, Boucherville, Québec, Canada J4B 6Y4

Abstract

Using a novel laser ultrasonics technique in situ measurements of austenite grain growth were conducted during continuous heating ($10 \, °C \, s^{-1}$) and subsequent isothermal holding at various temperatures in the range 950–1250 °C in a microalloyed linepipe steel. Based on the experimental results, a grain growth model was developed, which includes the pinning effect of precipitates present in the steel. Analyzing the grain growth behaviour and using the advanced thermo-kinetic software MatCalc, an approach was developed to estimate the initial distribution of precipitates in the as-received material and their dissolution kinetics. The evolution of the volume fractions and mean particle sizes of NbC and TiN leads to a time-dependent pinning pressure that is coupled with the proposed grain growth model to successfully describe the observed kinetics of austenite grain growth. The predictive capabilities of the model are illustrated by its application to independent grain growth data for rapid heat treatment cycles that are typical of the weld heat affected zone.
© 2011 Acta Materialia Inc. Published by Elsevier Ltd. All rights reserved.

1. Introduction

Grain size is an important factor in determining the strength and toughness of a material. In steels austenite grain size is a microstructural parameter that must be carefully controlled during hot working operations (e.g. hot rolling) and heat treatment, including those in the heat affected zone (HAZ) of welds. The austenite grain size resulting from these thermal or thermo-mechanical processes provides the initial condition for the subsequent phase transformation during cooling and thus affects the final microstructure and resulting mechanical properties [1,2]. For instance, increasing the austenite grain size shifts the continuous cooling transformation diagram to longer

reaction times, thereby increasing the possibility of martensite formation. Large austenite grain sizes are of particular concern during welding where the HAZ experiences rapid thermal cycles with high peak temperatures which give rise to austenite grain growth, especially in the region adjacent to the fusion zone. Martensite formation in this coarse grain region may lower the weld toughness and increase the risk of hydrogen cracking [3–8]. It also has an impact on the vulnerability to cold cracking and reheat cracking of welds. Further, grain growth in the HAZ influences the grain size in the weld metal, where the grains grow epitaxially from the HAZ [1].

The addition of small amounts of grain refining elements such as niobium, titanium, vanadium or aluminium can be used to control austenite grain growth during hot rolling, welding or heat treatment. The addition of these elements can result in finely dispersed particles which retard austenite grain growth [9–11]. During the fabrication of steels (i.e.

* Corresponding author. Tel.: +1 604 8222610; fax: +1 604 8223619.
E-mail address: mehran.maalekian@ubc.ca (M. Maalekian).

thermal or thermo-mechanical treatment) formation (nucleation and growth), coarsening or dissolution of these particles may occur. The associated evolution of particle size and volume fraction leads to a change in pinning force, which plays an important role in controlling the austenite grain size. Over the years a considerable amount of research work has been carried out on austenitization and the quantitative description of the retardation of grain growth by second phase particles [9,10,12–18]. In classical austenite grain growth tests a steel sample is heated from room temperature to a selected austenitizing temperature and held there for times (e.g. 30 min) that are usually much longer than the heating times. The observations made in these quasi-isothermal tests led to the introduction of the so-called grain coarsening temperature, above which significant austenite grain growth is observed. In many cases abnormal grain growth occurs in the region of the grain coarsening temperature, indicating that the dissolution of precipitates promotes grain growth. These studies have immediate relevance for selecting suitable reheat temperatures for industrial processes (e.g. in a hot mill). However, in many industrial processes austenite grain growth occurs under conditions where the non-isothermal character of the heat treatment path cannot be neglected; the HAZ is the most prominent example of this situation.

A number of attempts have been made to study the effect of heating rate and more complex non-isothermal heat treatment cycles on austenite grain growth kinetics [2,7,8,15,19–23]. An extensive review of non-isothermal grain growth was published by Mishra and DebRoy [24]. Militzer et al. [2] studied the effect of particle pinning pressure on austenite grain growth by analyzing a pinning parameter, which was determined using the limiting grain size as a function of heating rate and soaking temperature. By investigating isothermal austenite grain growth and the particle coarsening behaviour Moon et al. [23] quantified the effects of particles on grain boundary pinning and alloying elements on grain boundary mobility. Employing the additivity rule, austenite grain growth was simulated for non-isothermal conditions in the weld HAZ of a Ti microalloyed steel. Based on elementary kinetic models of grain growth and carbide dissolution integrated over the weld cycle, Ashby and Easterling [7] proposed grain growth diagrams for steel welding by fitting the unknown kinetic constants to data from real or simulated welds. Their analytical model was further improved by incorporating precipitate coarsening [8]. Andersen and Grong [15] proposed an extensive analytical model of grain growth in the presence of growing and dissolving precipitates. In their approach a differential grain growth equation, which can be integrated in temperature–time space, was used to calculate the mean grain size for fixed starting conditions. Particle coarsening was described using the differential formulation of the classical Lifshitz–Slyovoz–Wagner (LSW) theory [25,26] for continuous heating and cooling conditions. The rate of particle dissolution was modelled using the so-called invariant field solution approach first developed analytically by Whelan [27] and treated numerically by Ågren [28]. In the model there is no impingement of diffusion fields from neighbouring precipitates. Andersen and Grong presented their results in the form of mechanism maps which show the competition between the various processes during grain growth in conjunction with coarsening or dissolution of precipitates.

Recently, Banerjee et al. [29] investigated the effect of high heating rates (up to 1000 °C s^{-1}) and various austenitizing temperatures on the non-isothermal austenite grain growth kinetics in a Nb–Ti microalloyed linepipe steel. Austenite grain sizes were measured using metallographic techniques and they also studied the particle size distribution in the as-received and continuously heated steel by transmission electron microscopy (TEM). Using thin foils and a replica technique, energy-dispersive X-ray (EDX) and selected area diffraction pattern (SADP) analyses of precipitates in the steel investigated showed that precipitates are randomly distributed and can be divided into three families, i.e. Ti-rich, Nb-rich and Mo-rich, with sizes ranging from 1 to 200 nm. Further, a detailed analysis revealed two populations of Nb-rich precipitates, i.e. small (<5 nm) and large particles (>10 nm), in the as-received material. According to the processing route of the steel, which is composed of casting, hot rolling (in the austenite region) and coiling in the temperature range 550–600 °C, it is assumed that large Nb-rich particles precipitated in austenite during hot rolling [30], whereas the fine Nb-rich particles formed in ferrite during coiling [31]. This is consistent with the crystallographic orientation of the fine Nb(CN) precipitates with the ferrite matrix, as investigated by Banerjee et al. [29]. The well-known Baker–Nutting relationship [42] was found, indicating that the fine Nb-rich particles had been formed during the coiling process. Based on the experimental observations, a phenomenological grain growth model was proposed by coupling the grain growth kinetics with the dissolution kinetics of Nb(CN) [29].

Although significant progress has been made, most of the quantitative description of non-isothermal grain growth is based on isothermal grain size measurements on post-processing specimens with very limited information on the evolution of the grain structure during processing. With conventional approaches (e.g. metallography) in situ monitoring of austenite grain growth at high temperatures is impossible. Further, in some cases revealing austenite grain boundaries post processing in low carbon steels is very challenging, if not impossible. An emerging alternative technique is laser ultrasonics [32,33]. The laser ultrasonics methodology recently developed specifically for metallurgical applications is a unique technique which allows in situ measurement of austenite grain size evolution with very good time resolution [34–37]. Further, just one test provides the entire grain growth curve for a given thermal cycle, whereas metallographic investigations would require a multiplicity of labour intensive examinations to obtain this curve. The data acquisition rate for laser

ultrasonics can be as high as 50 Hz, thereby enabling the rapid capture of microstructure evolution, e.g. during heat treatment cycles replicating those occurring in the HAZ, which may be elusive by conventional metallography. For example, in the continuous heating studies of Banerjee et al. [29] the times at peak temperatures of approximately 0.5 s before starting the quench are comparable with the heating times in austenite at the highest employed heating rate of 1000 °C s^{-1}.

In this paper the study of austenite grain growth kinetics in the microalloyed X-80 steel grade previously investigated by Banerjee et al. [29] has been extended using the laser ultrasonic technique as the grain size measurement tool. Based on the experimentally measured limiting grain sizes at various reheat temperatures an approach is proposed to evaluate the initial precipitate distribution in the as-received material. To simulate the austenite grain growth behaviour a grain growth model is coupled with the thermo-kinetic software MatCalc (http://www.matcalc.at). This coupling enables integration of the precipitate kinetics with the grain growth model in a more generalized way than that proposed in the phenomenological model of Banerjee et al. [29].

2. Experimental procedure

The steel studied is an X-80 microalloyed linepipe steel with the chemical composition of 0.06 C, 1.65 Mn, 0.034 Nb, 0.012 Ti, 0.24 Mo, 0.005 N (key alloying elements in wt.%). The microstructure of the as-received steel was investigated by optical microscopy. The specimen was polished using conventional metallographic techniques and then etched in 2% Nital solution. In addition, LePera etching was employed to reveal islands of remaining austenite and/or martensite. For austenite grain growth studies sheet specimens were used of 10 mm width, 1.5 mm thickness and 60 mm length (see Fig. 1). The surfaces of the samples in the measurement area were machined to a smooth finish to minimize the effect of surface roughness on ultrasound attenuation. The specimens were heat treated in a Gleeble 3500 thermo-mechanical simulator equipped with a laser ultrasonics system. The tests were performed under an argon atmosphere to minimize surface oxidation. The

temperature was controlled using an S-type (Pt–Pt/10%Rh) thermocouple spot welded to the centre of the sample. The specimens were heated at a rate of 10 °C s^{-1} to various soak temperatures (i.e. 950 °C, 1050 °C, 1150 °C, 1200 °C and 1250 °C). After holding for about 15–20 min the samples were naturally cooled. Water quenching was utilized when rapid cooling was required for metallographic measurement of the grain size.

Laser ultrasonics is based on the generation of ultrasonic waves by a pulsed laser and the subsequent detection of these waves by a laser interferometer. Analysis of the detected ultrasonic pulse provides microstructural information. The ultrasound velocity is, for example, a direct measure of the elastic modulus, which depends on temperature, crystal structure and texture. The decay of an ultrasonic wave depends on scattering by the microstructure (i.e. by the bulk of the grains) and internal friction. Attenuation of the waves can be directly correlated with grain size. Laser ultrasonics is a remote, continuous and non-destructive technique that can be operated in situ at high temperatures for bulk observations [34–37]. In the present investigation the ultrasonic waves were generated using a frequency doubled Nd:YAG laser with a short (5 ns) and energetic (150 mJ) green (532 nm) light pulse. The light pulse generates a wideband ultrasound wave by ablating a thin surface layer. As the ultrasonic wave propagates through the material it is scattered by discontinuities such as grain boundaries and so looses a fraction of its amplitude. The unscattered component travels through the thickness and then is reflected back to the original surface. The reflected wave is detected using a laser interferometer employing a longer pulse duration (50 μs) and lower pulse energy (70 mJ) frequency stabilized infrared (wavelength 1064 nm) Nd:YAG laser especially developed for this application. The acquisition rate was initially set to 10 Hz, to capture the rapid change in grain size during heating, and was gradually lowered to about 0.5 Hz during isothermal holding at the soak temperature. Fig. 1 shows schematically the experimental set-up. The details of the laser ultrasonic measurement technique and its experimental validation can be found elsewhere [37–39]. The quantification of grain sizes is based on a calibration made using metallographically measured average equivalent area diameters (EQAD) for complex phase (CP) and X-80 steels [38]. Here all grain sizes are reported as mean volumetric grain sizes that can be obtained by multiplying the mean EQAD by 1.2, as proposed by Giumelli et al. [18].

To verify the laser ultrasonic data the austenite grain size was metallographically measured in selected cases of as-quenched samples. The prior austenite grain boundaries were revealed using 3 ml dodecylbenzene sulfonate and 0.2 g copper chloride in 100 ml saturated aqueous picric acid in the presence of 2 ml Triton X-100 surface active reagent. The optimized temperature and time for etching were 90 °C and 20–25 s, respectively. To estimate the degree of precipitation in the as-received material a series of ageing tests were conducted at 600 °C using a conventional furnace
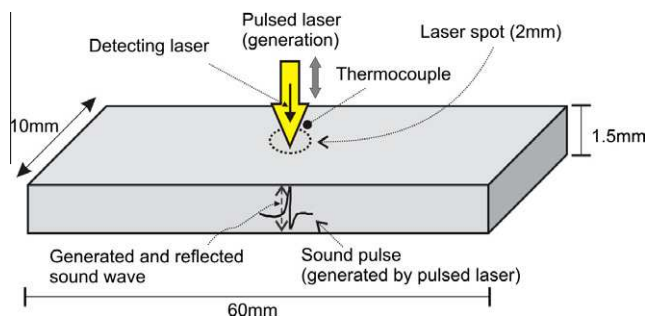

Fig. 1. Schematic diagram of the specimen geometry and the laser ultrasonics experimental set-up.

with an Ar atmosphere. The variation in hardness with time was recorded using Vickers microhardness (500 g load) measurements.

3. Experimental results

3.1. Initial microstructure and second phase particles

The microstructure of the as-received steel is shown in Fig. 2. The microstructure mainly consists of polygonal ferrite, acicular ferrite (see Fig. 2a) and martensite–austenite islands (see Fig. 2b). Information on precipitates in the X-80 steel investigated is available from the TEM studies of Banerjee et al. [29]. However, these TEM studies do not provide measured data for the volume fraction of precipitates. Thus ageing tests in combination with hardness measurements were conducted in the as-received material to provide information on the extent of precipitate strengthening, and also indirectly to some degree on the precipitation kinetics during ageing [40]. For the as-received material only softening was observed, indicating that no substantial

formation of new precipitates occurred. Therefore, it is assumed for the present analysis that all microalloying elements had already been precipitated in the as-received steel and the precipitation state is close to the equilibrium condition.

3.2. Austenite grain growth

Fig. 3 shows the austenite grain size evolution in the X-80 steel obtained in situ by the laser ultrasonic technique at a $10 \, °C \, s^{-1}$ heating rate followed by various isothermal holding temperatures. In this graph time zero corresponds to the sample reaching 900 °C. For comparison with laser ultrasonic grain sizes Fig. 3 also shows metallographically measured grain sizes for 1050 °C, 1150 °C and 1250 °C at selected soaking times. Examples of optical micrographs for these metallographic studies are given in Fig. 4.

The laser ultrasonic measurements provide a wealth of data points during the heating and subsequent isothermal holding stages. The ultrasonic data show some scatter at any test temperature. The reproducibility of these measurements is, however, at least as good as that of metallographic techniques to measure austenite grain size, as verified by previous validation studies [39,41]. A further indication of the good reproducibility of the data in the present case is the overlap of the laser ultrasonic curves during the early stages of heating. In addition, the absolute value of grain size measured by laser ultrasonics agrees relatively well with the metallographically obtained grain size.

The laser ultrasonic curves reach a plateau for a sufficiently long period of isothermal holding (see dashed lines in Fig. 3), indicating that a limiting grain size is attained. Quantitative agreement between the metallographically and laser ultrasonically determined grain sizes was obtained within the errors of measurement for four out of the five cases investigated here. For the case of 1 min holding at 1150 °C the average metallographic grain size
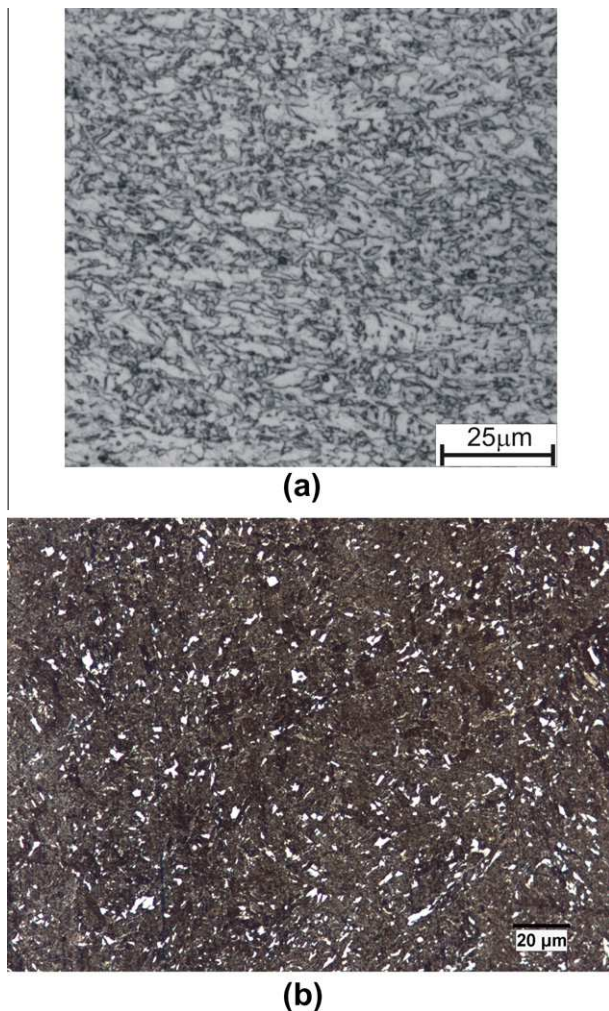

Fig. 2. Optical micrographs of the as-received X-80 steel: (a) Nital etch, (b) LePera etch to reveal martensite–austenite islands (shown in white).
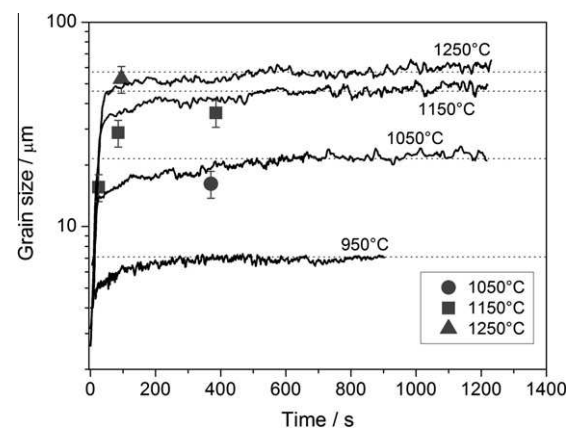

Fig. 3. Austenite grain growth behaviour measured by laser ultrasonics at $10 \, °C \, s^{-1}$ heating rate followed by isothermal holding. Time zero corresponds to 900 °C, and symbols are average volumetric grain diameters obtained from the EQAD as measured by metallography. Dashed lines show the limiting grain sizes.
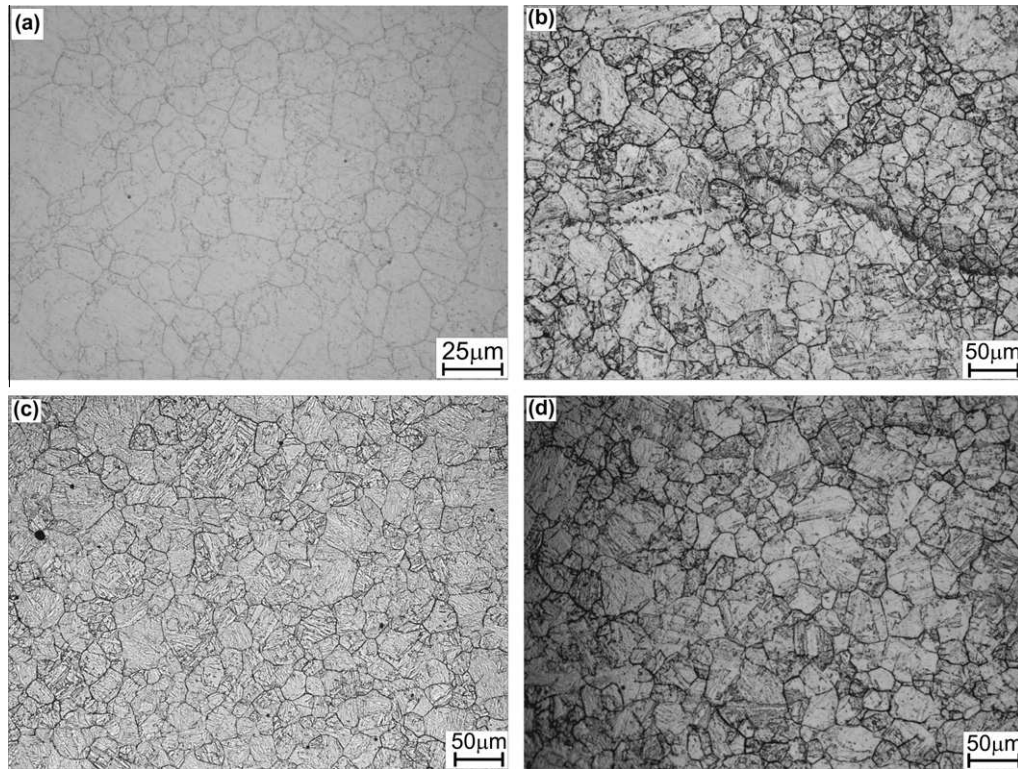
Fig. 4. Optical micrographs of prior austenite grain boundaries for a 10 °C s⁻¹ heating rate followed by subsequent isothermal holding: (a) 6 min at 1050 °C; (b) 1 min at 1150 °C; (c) 6 min at 1150 °C; (d) 1 min at 1200 °C.

is somewhat smaller than the apparent laser ultrasonic grain size. In this case (see Fig. 4b) the grain structure displays a broader distribution of grain sizes compared with the more homogeneous grain structures for holding times of 6 min at 1050 °C and 1150 °C and 1 min at 1200 °C. This may be indicative of abnormal grain growth taking place in the early stages of holding at 1150 °C, presumably due to dissolution of NbC (and Nb(C,N)). Since large grains dominate the laser ultrasonic response, i.e. the attenuation caused by scattering is dominated by the material having the larger grain size [38], the apparent laser ultrasonic grain size is larger than the metallographically determined average grain size. Nevertheless, after sufficient holding at 1150 °C, when all NbC particles are dissolved, normal grain growth resumes to reach a limiting grain size due to the presence of a population of stable TiN precipitates.

4. Model

4.1. Grain growth model

The in situ experimental measurements of austenite grain size show a limiting grain size at each isothermal holding temperature, confirming that grain growth stops due to the presence of stable second phase particles. To quantify this effect the volume fraction and particle size must be determined. The evolution of these precipitates (i.e. dissolution or coarsening) during heat treatment has a significant effect on the kinetics of austenite grain growth

and the limiting grain size. Thus to describe austenite grain growth a grain growth model must be developed that accounts for the evolution of the precipitates and their pinning forces on grain boundaries.

The driving pressure for grain growth is given by [43,44]

$$P_d = \alpha \frac{\gamma}{D} \tag{1}$$

where D is the mean volumetric grain diameter, γ is the grain boundary energy, which is assumed to be 0.5 J m⁻² [45], and α is a dimensionless geometric constant. For grain growth in three dimensions, as investigated in the present study, $\alpha = 4$ [46].

Second phase particles that are present in the matrix due to microalloying with Ti and Nb retard austenite grain growth. The austenite grain boundaries are pinned by these precipitates, slowing or even inhibiting their movement during thermal treatment. The pinning force is governed by the volume fraction of the particles (f) and their size (mean particle radius r). The well-known Zener pinning pressure exerted by second phase particles on grain boundary is expressed by [47]

$$P_z = \beta \frac{\gamma \cdot f}{r} \tag{2}$$

where β is a dimensionless constant [9,10,48] and $\beta = 12$ according to Rios [48].

The grain boundary moves with a velocity (v) in response to the net driving pressure ($\Delta P = P_d - P_z$) on the boundary. It is generally assumed that the velocity is

directly proportional to the driving pressure, the constant being the effective mobility (M) of the boundary, i.e. [45]

$$v = M\Delta P \tag{3}$$

The grain boundary velocity can also be expressed by

$$v = \frac{1}{2}\frac{dD}{dt} \tag{4}$$

where t is the time. Assuming that the mobility is given by an Arrhenius relationship and combining Eqs. (1)–(4) the differential equation for grain growth is obtained:

$$\frac{dD}{dt} = M_0 \exp\left(-\frac{Q}{RT}\right) \cdot \gamma\left(\alpha\frac{1}{D} - \beta\frac{f}{r}\right) \tag{5}$$

Here M_0 is the pre-exponential mobility factor, Q is the apparent activation energy of the mobility, T is the temperature and R is the universal gas constant. In this work an activation energy of $Q = 350$ kJ mol^{-1} is used, which was determined by multiple regression analysis for several Nb-containing steels by Uhm et al. [49]. The mobility factor M_0 is a scaling parameter which can be determined from a limited number of experimental grain growth data. Here $M_0 = 120$ m^4 J^{-1} s^{-1}, taken from Banerjee et al. [29], was used for the present X-80 steel.

4.2. Precipitation model

Classical concepts for precipitate nucleation and growth have been developed for binary systems [50], however for multi-component systems it is more challenging to deal with the local equilibrium conditions for the chemical potentials across the interface. An alternative treatment of precipitate growth has recently been presented, which is suitable for application to multi-component systems [51–53]. The model is based on Onsager's thermodynamic extremal principle in which any non-equilibrated thermodynamic system evolves along the particular kinetic path where entropy production is a maximum [50–52]. For the modelling of the precipitation behaviour in the present microalloyed steel, this method is used and has been implemented in the thermo-kinetic software MatCalc (version 5.40) (http://www.matcalc.at).

The total Gibbs free energy G of the system with n components and m precipitates can be expressed as [51]

$$G = G_m + \sum_{k=1}^{m}\frac{4\pi\rho_k^3}{3}\left(\sum_{i=1}^{n}c_{ki}\mu_{ki}\right) + \sum_{k=1}^{m}4\pi\rho_k^2\gamma_k \tag{6}$$

where the first term is the Gibbs free energy of the matrix, the second term is the bulk free energy of all precipitates, and the last term takes into account the energy contribution of the precipitate–matrix interfaces. In Eq. (6) μ_{ki} is the chemical potential of component i in precipitate k, c_{ki} is the mean concentration of element i in precipitate k, ρ_k is the radius of precipitate k, and γ_k is the interfacial energy of the precipitate–matrix interface. These interfacial energies are obtained from a nearest neighbour broken bond model [54]. The Gibbs free energies are calculated using the standard CALPHAD method and the associated thermodynamic database [55].

If the system is not in equilibrium a driving force exists to produce variation in the independent state parameters ρ_k and c_{ki} to decrease the total free energy of the system. In the present paper constant precipitate compositions are assumed such that only the evolution of the precipitate radii by multi-component diffusion in the matrix is considered. An important feature of MatCalc is that, in following the evolution of numerous precipitate classes simultaneously, information on the evolution of the size distribution of the precipitates is obtained [50]. In the software the nucleation kinetics of precipitates is calculated from classical nucleation theory (CNT) [56] extended to multi-component systems [50]. Growth and/or dissolution of precipitates of each size class are then evaluated based on a set of linear differential equations for the radii of the precipitates derived by Svoboda et al. [51] assuming that the spherical precipitates are randomly distributed in a homogeneous matrix.

The numerical time integration of evolution equations is performed by the software using the classical Kampmann–Wagner approach [57]. In this approach in every time interval (simulation time is divided into discrete time intervals) a precipitate class may be created (nucleation and growth stages) or removed (dissolution stage), and the growth kinetics of the existing precipitate classes are evaluated. For the present calculations the thermodynamic database 'mc_steel' [55] and the diffusion database 'mc_sample_Fe' [50] are employed as provided by the software. The diffusivity of the microalloying elements (Nb and Ti) in austenite according to the database are: D_{Nb} (m^2 s^{-1}) $= 4.2 \times 10^{-4}$ exp(-286 kJ mol$^{-1}/RT$) and $D_{Nb} = 1.5 \times D_{Ti}$. The initial volume fractions and particle sizes must be generated first with MatCalc. Generation of the precipitate data was carried out by taking 100 particle size classes for each precipitate family and performing a hypothetical heat treatment cycle that qualitatively resembles the processing route of the steel. An increase in the number of size classes increased the computational time with no change in the precipitation kinetics, indicating that the selected number of size classes provides a sufficient representation of the particle size distribution in the system investigated. Further details of the model and the numerical treatment of the evolution equations are given in the works of Kozeschnik and co-authors [50–53].

5. Modelling results

As shown by Banerjee et al. [29], the steel contains a fine dispersion of a number of complex precipitates containing Ti, Nb and Mo. Here, to simplify the calculation, the precipitates are divided into three stoichiometric families, i.e. TiN, NbC and Mo$_2$C. The equilibrium thermodynamic calculations using the MatCalc software, shown in Fig. 5, indicate that Mo$_2$C particles will dissolve at 670 °C, whereas the solution temperatures for the NbC and TiN
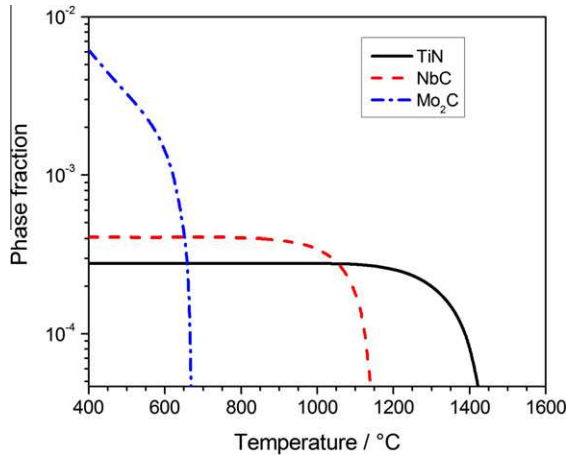
Fig. 5. Stability of the precipitates (TiN, NbC and Mo$_2$C) in the X-80 steel with respect to temperature calculated in the equilibrium state (i.e. infinitely large precipitates) using MatCalc.
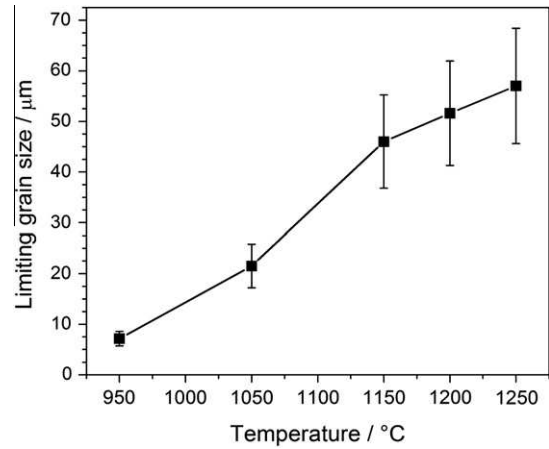

Fig. 6. Measured limiting grain sizes at different temperatures. The accuracy of the grain size measurements is about 20%, as shown by the error bars.
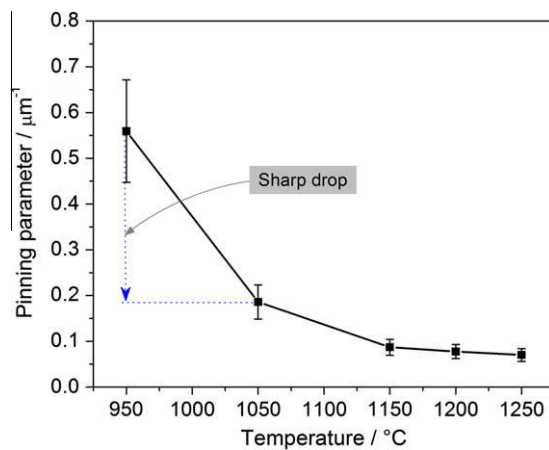

Fig. 7. Pinning parameter versus temperature calculated based on D_{lim}.

precipitates are 1156 °C and 1450 °C, respectively. Therefore, for the evaluation of austenite grain growth it is assumed that all Mo$_2$C precipitates are in solution, whereas evolution of the TiN and NbC precipitates are considered in the grain growth model.

For the grain growth model the initial volume fraction (f) and mean radius (r) of the precipitates are required. Consistent with the ageing experiments, it is assumed that all Ti and Nb is precipitated as TiN and NbC, respectively, in the as-received material. The volume fractions of the precipitates are determined to be $f_{TiN} = 0.00022$ and $f_{NbC} = 0.00038$, respectively. In order to convert phase fraction (mol_p) to volume fraction (f_p), conversion factors of 0.80 and 0.94 are used for TiN and NbC, respectively. These are obtained from: $f_p = \frac{1}{2} mol_p \times \frac{M_p/\rho_p}{56/\rho_{Fe}}$, where M_p and ρ_p are the atomic weight and the density of the precipitates (NbC or TiN), respectively, and ρ_{Fe} is the density of Fe.

The initial radii of the precipitates can be estimated by simulating the dissolution kinetics at each holding temperature to replicate the values of the limiting grain sizes as well as the kinetics, i.e. the holding times, to reach them as measured by laser ultrasonics. Therefore, the limiting grain sizes are plotted against the reheat temperature in Fig. 6. From Eq. (5) the rate of grain growth becomes zero when the limiting grain size (D_{lim}) is approached, i.e. at $D = D_{lim}:dD/dt = 0$. Therefore, the pinning parameter ($P_p = 12f/r$) can be written in terms of D_{lim} as:

$$P_p = \frac{4}{D_{lim}} \qquad (7)$$

Using Eq. (7) the pinning parameter is calculated as a function of temperature, as illustrated in Fig. 7. Due to dissolution and/or coarsening of the precipitates the pinning parameter decreases with temperature. In the presence of multiple particle distributions the pinning parameter can, as a first approximation, be expressed by [29]:

$$P_p = \beta \cdot \sum_i \frac{f_i}{r_i} \qquad (8)$$

where the summation index i represents all present particle families, i.e. here TiN and small and large NbC. To calculate the pinning parameter (Eq. (8)) the average particle size is considered, which is extracted from the particle size distribution calculated with MatCalc.

At 1250 °C all NbC precipitates are expected to dissolve, whereas most TiN remains as a precipitate. The slight decrease in the pinning parameter when the temperature increases from 1150 °C to 1250 °C (see Fig. 7) may be related to minor dissolution of the TiN precipitates (see Fig. 5) which can be neglected as a first approximation. Thus the pinning pressure at 1250 °C, which is only related to the presence of TiN particles, can be utilized to estimate the mean radius of the TiN particles as follows:

$$P_p = \beta (f/r)_{TiN} = 12(0.00022/r_{TiN}) \approx 0.07 \ \mu m^{-1} \rightarrow r_{TiN}$$

$$\approx 38 \ nm$$

Simulations with MatCalc confirm that neither coarsening nor significant dissolution occur within 20 min at 1250 °C for a TiN particle distribution with an average radius of 38 nm. Using the information on TiN, the sizes

and volume fractions of the two populations of NbC precipitates (i.e. the fine and large ones) in the as-received material can be estimated from the grain growth kinetics at 950 °C, 1050 °C and 1150 °C. As the total volume fraction of NbC has already been determined ($f_{NbC} = 0.0038$), there are three remaining parameters to characterize these two populations, i.e. the mean radii, $r_{NbC(large)}$ and $r_{NbC(small)}$, of the small and large NbC precipitates and the volume fraction, $f_{NbC(large)}$, of the large NbC precipitates. The observation of a limiting grain size indicates equilibrium precipitation condition for the given temperature. Fig. 7 shows a significant decrease in the pinning parameter between 950 °C and 1050 °C ($P_p = 0.18 \ \mu m^{-1}$), suggesting that, as a first approximation, the fine NbC particles ($NbC_{(small)}$) are dissolved at this temperature. Initial values for the three unknowns can be selected under the assumption that $f_{NbC(large)}$ represents the equilibrium volume fraction of NbC at 1050 °C, i.e. 0.00027, and all NbC remains precipitated at 950 °C. To fit the observed pinning parameters at 950 °C and 1050 °C the initial values for the radii of the large and small NbC precipitates are 28 and 3.7 nm, respectively. These values provide the starting point for an iterative estimation of the NbC particle size distribution in the as-received material. In this iterative process the measured grain growth kinetics are taken into account such that the dissolution times of the precipitates match the holding times to reach the limiting grain size. The flow chart shown in Fig. 8 summarizes the approach to estimating the volume fractions and particle sizes of the two populations of NbC ($NbC_{(small)}$ and $NbC_{(large)}$) based on the measured evolution of grain size.

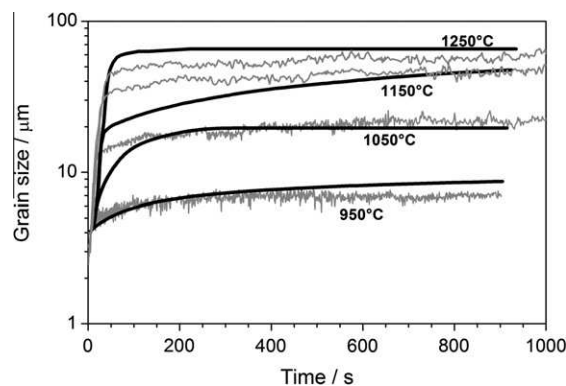Fig. 9 compares the austenite growth kinetics calculated using the above methodology with that measured by laser

Fig. 9. Austenite grain growth kinetics at a $10 \ °C \ s^{-1}$ heating rate followed by isothermal holding: calculated (black lines) and measured by laser ultrasonics (grey lines). Time zero corresponds to 900 °C.

ultrasonics. The calculated austenite grain growth kinetics are in reasonable agreement with the experimental data at all temperatures studied. This indicates that the present grain growth model can reasonably capture the kinetics of grain growth during continuous heating and isothermal holding.

Fig. 10 shows the particle size distributions in the as-received steel obtained using MatCalc with the present approach (see Fig. 8). Since analysis of the grain growth kinetics (Eq. (5)) is based on the mean precipitate data, Table 1 shows the estimated mean size, volume fraction and number density of the three precipitate populations.

The kinetics of evolution of the precipitates for the heating rate of $10 \ °C \ s^{-1}$ and subsequent isothermal holding at different soak temperatures are shown in Figs. 11 and 12. The calculation shows that the small NbC particles dissolve
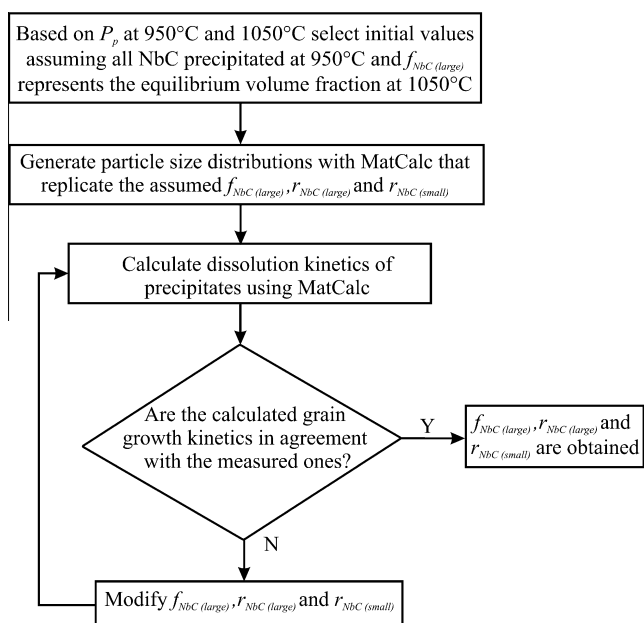

Fig. 8. Systematic steps to estimate volume fractions and particle sizes of NbC based on the measured grain sizes.
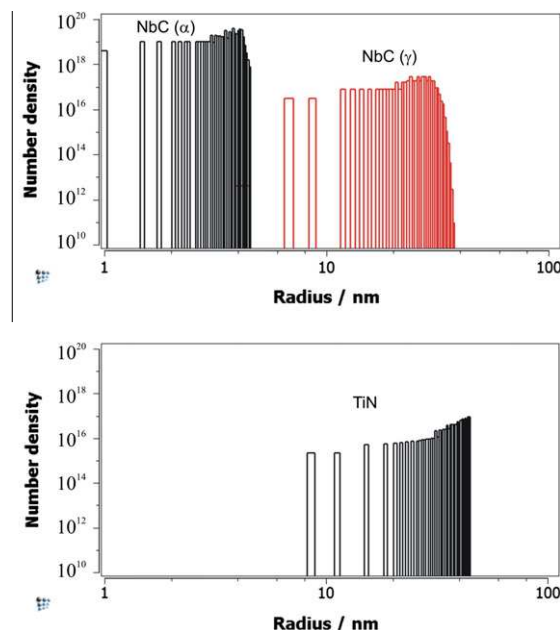

Fig. 10. Bimodal (NbC) and monomodal (TiN) size distributions of precipitates with average radii of 3.5, 24 and 38 nm, respectively, in the as received X-80 steel generated using MatCalc.

Table 1
Estimated mean values of the initial precipitate parameters.

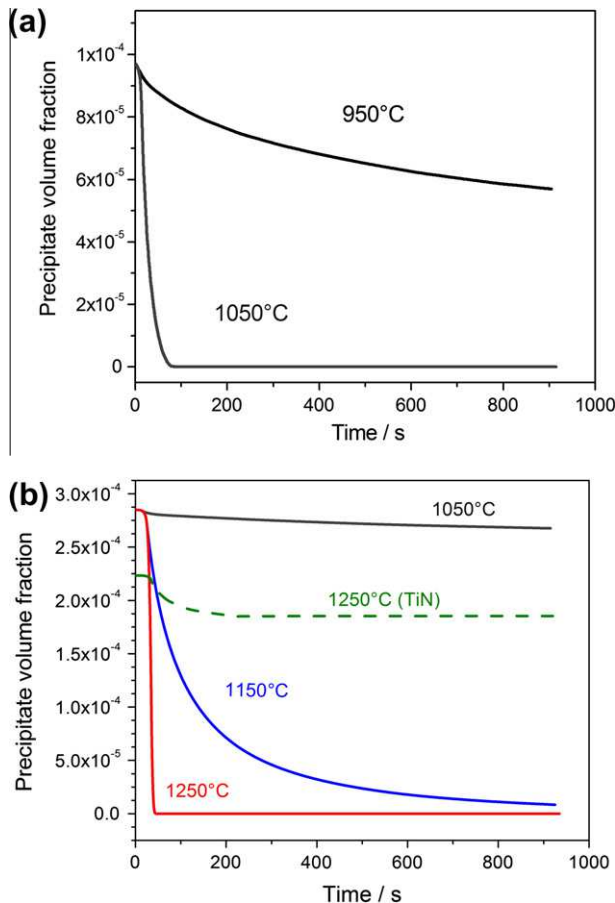| Precipitate	Volume fraction	Mean radius (nm)	Number density (m^{-3})
TiN	2.2×10^{-4}	38	1.1×10^{18}
NbC$_{large}$	2.8×10^{-4}	24	4.4×10^{18}
NbC$_{small}$	1.0×10^{-4}	3.5	5.6×10^{20}

Fig. 11. Dissolution kinetics of (a) small and (b) large NbC precipitates in X-80 steel heated at 10 °C s^{-1} and held at different soaking temperatures. The dashed line in (b) shows the dissolution kinetics of TiN precipitates at the highest temperature (1250 °C). Time zero corresponds to 900 °C.

Fig. 12. Mean particle sizes calculated for a 10 °C s^{-1} heating rate and subsequent holding at 1250 °C.

NbC commences, whereas the change in size of TiN precipitates is negligible.

6. Discussion

The calculated grain growth kinetics show that a limiting grain size is reached within approximately 1 min for holding temperatures of 1050 °C and 1250 °C. This can be attributed to the rapid dissolution of small NbC at 1050 °C (Fig. 11a) and large NbC at 1250 °C (Fig. 11b). The limiting grain size at 1250 °C is slightly overpredicted, since the precipitation model predicts some minor dissolution of TiN that was neglected when estimating the initial TiN particle radius. Similarly, at 950 °C the model predicts some minor grain growth for some holding times when experimental data indicate that a limiting grain size has already been reached. Here the precipitation model predicts a very slow dissolution of small NbC particles, whereas the observation of a limiting grain size in the measurements would suggest that a stable particle size distribution is established more quickly. For those particles with sizes in the range 1–5 nm (see Fig. 10) the solubility limit is significantly affected by the Gibbs–Thomson effect, such that the predicted dissolution kinetics depend in detail on the value of the interfacial energy and the particle size distribution selected. In the present case the volume fraction of the small particles decreases by about 40% (see Fig. 11a) to reach the solubility limit for the smallest size class (1 nm) in the distribution. The associated evolution of the pinning pressure leads to simulated grain growth kinetics that agree with the measurements, within the experimental error. For example, the calculated limiting grain size is 8 μm, whereas the measured one is 7 μm.

At 1150 °C the calculated and measured limiting grain sizes are in agreement, but the apparent grain growth kinetics both measured and calculated are of limited value because abnormal grain growth occurs at this temperature (see Fig. 4b). This is a result of gradual dissolution of the coarse NbC particles at 1150 °C, as shown in Fig. 11b.

very quickly at all temperatures except for the lowest temperature of 950 °C, at which dissolution is very slow (see Fig. 11a). In contrast, the coarse NbC precipitates are more stable as they do not dissolve at 950 °C and only slightly dissolve at 1050 °C, as shown in Fig. 11b. However, they dissolve almost completely at 1150 °C after a sufficiently long holding time and the dissolution rate becomes faster at higher temperatures. At the highest temperature (1250 °C) TiN particles dissolve only slightly (the associated change in the pinning parameter is 0.01 μm^{-1}). The calculated mean particle sizes associated with dissolution of the two types of NbC as well as the minor dissolution of TiN precipitates are shown in Fig. 12. It shows that all small NbC is dissolved before dissolution of the larger
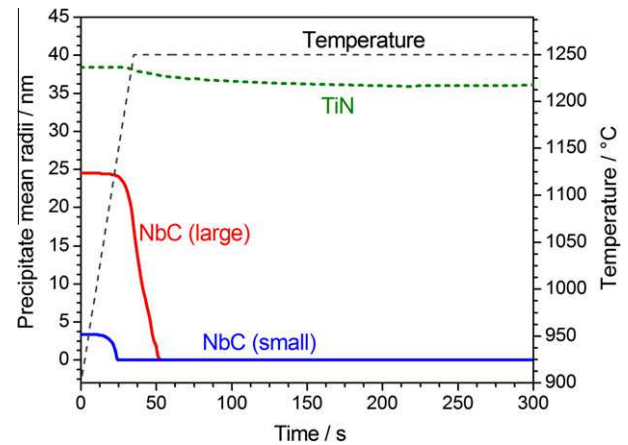
As a result, the model that considers just a mean grain size predicts continuous effective grain growth. Similarly, the laser ultrasonic grain size is an effective grain size that, as discussed earlier, is biased towards the larger grains in the distribution. As soon as the large NbC precipitates are completely dissolved normal grain growth resumes and the laser ultrasonic grain size corresponds to measurement of the average grain size as simulated by the model. In other words, both the laser ultrasonic measurements and the average grain size model presented in this work are only applicable when normal rather than abnormal grain growth occurs.

The mean radii estimated from the present limiting grain sizes and grain growth analyses are of the same order of magnitude but differ in detail from those obtained based on TEM studies by Banerjee et al. [29], i.e. 61 nm for TiN, 69 nm for large NbC and 2 nm for small NbC. Even though direct measurement of the particle sizes would be preferred, it must be noted that extensive TEM analysis would be required to obtain reliable data on particle sizes. In the previous study Banerjee et al. [29] used the replica technique to measure the sizes of the coarse precipitates, but only particles with radii >10 nm could be analyzed, and this may have led to an overestimation of their average size. Further, the size of the small Nb precipitates was estimated from a limited number of thin foil observations. The proposed approach of estimating the average size of precipitates is a convenient method that may be an efficient tool when considering pinning for grain growth simulations. Using this approach the amount of extensive and time consuming TEM work can be reduced. However, limited amount of TEM information is required to validate the basic assumptions of the model, i.e. what precipitate families are present and an order of magnitude estimate of the typical precipitate sizes.

The proposed austenite grain growth model has been established for a slow heating rate (10 °C s^{-1}) and long isothermal holding, however, an important aspect of non-isothermal grain growth studies is to capture the grain growth kinetics during rapid heating cycles that are typical for the HAZ. Thus the predictive capabilities of the proposed model are examined using the independent grain growth study of Banerjee et al. [29] for selected rapid heat treatment cycles. Based on their experimental results they proposed a simple mean field dissolution model for the average particle size coupled with the grain growth model. In their model the mean sizes of the NbCN and TiN particles were used as determined from TEM observations. Neither particle size distribution nor particle coarsening were considered. The present MatCalc simulations confirm that coarsening is negligible for all heat treatments investigated. Using the present data for the precipitates (the size and volume fractions as well as diffusion and thermodynamic data) the present model was examined as was the model of Banerjee et al. [29] for these rapid heating conditions. For this purpose model predictions for continuous heating with a 0.5 s holding time at the peak temperature are

compared with the experimental data of Banerjee et al. [29]. Fig. 13 compares the measured austenite grain sizes as a function of heating rates and peak temperatures with the simulated grain growth kinetics when different precipitation models are coupled with the grain growth model: (i) the present model with a particle size distribution; (ii) the original model of Banerjee et al. [29]; (iii) the simple mean field dissolution model of Banerjee et al. [29] in which the present sizes and volume fractions of precipitates as well as diffusion and thermodynamic data (that are consistent with MatCalc) are used. The solubility products of TiN and NbC obtained from the MatCalc thermodynamic database are $\log K_{TiN} = 4.65 - (15,326/T)$ and $\log K_{NbC} = 4.55 - (10,345/T)$. Also, a particle/matrix interfacial energy of 0.66 J m^{-2} is employed according to MatCalc. Considering that the present model has been calibrated with limiting grain sizes observed for long isothermal soaking times (15–20 min), very good agreement with the measured data for rapid heating is observed. The analysis indicates that for rapid heating cycles with short soaking times where particle coarsening is rather unlikely a simple mean field dissolution model would be sufficient to model the grain growth kinetics. The predictions for both models (i.e. the simple dissolution model and MatCalc) using the precipitate data from the present analysis provide a better description than the original simulation results of Banerjee et al. [29]. Further, their model fails to predict grain growth in heat treatment scenarios with long holding times, e.g. at 1250 °C, where only TiN particles are present. In this case the model of Banerjee et al. would yield, using the TEM data for precipitate sizes, a limiting volumetric grain size of 97 μm rather than the observed 65 μm. As a result, the proposed physically based austenite grain growth model successfully describes austenite grain growth in the presence of second phase particles for a wide range of thermal cycle scenarios from heat treatment (with s slow heating rate and a long holding time) to welding (with a rapid heating rate and a negligible hold time).
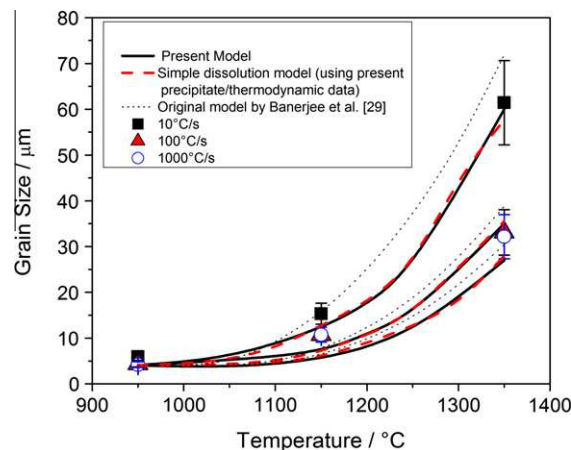

Fig. 13. Comparison between the predicted and measured austenite grain sizes for continuous heating (10, 100 and 1000 °C s^{-1}) followed by a short hold (0.5 s). The experimental data are taken from Banerjee et al. [29].

An integral part of the proposed model is prediction of the dissolution kinetics of precipitates. It may be possible to validate these predictions for the steel investigated where a variety of complex precipitates are present using dedicated continuous cooling transformation (CCT) studies. In particular, Nb in solution has a large effect in delaying austenite decomposition [6,58,59]. For this purpose phase transformation models are being developed that quantitatively account for the Nb level in solution [57]. Coupling such a transformation model with the present grain growth–precipitation model will provide a microstructure evolution model that can then be evaluated for selected heat treatment cycles based on the measured transformation kinetics and resulting final microstructures.

7. Conclusions

In the present work in situ laser ultrasonic austenite grain size measurements were employed to develop a combined grain growth–precipitation model. The temperature dependence of the limiting grain sizes and the holding times to reach them was used to estimate initial precipitate sizes and volume fractions using the thermo-kinetic simulation software MatCalc. Subsequently, it was shown that a simple mean field dissolution model that assumes a mean particle size can be coupled with the grain growth model rather than the more complex MatCalc approach that explicitly considers particle size distributions. Further, this simplified grain growth–precipitation model has been validated by predicting austenite grain growth for rapid heat treatment cycles that typically occur in the HAZ of welds. The predicted grain growth kinetics agree well with the grain sizes metallographically measured by Banerjee et al. [29].

The proposed methodology is a promising tool to establish austenite grain growth models for different steel chemistries with a reduced need for extensive metallographic and TEM studies. In addition, using the laser ultrasonic technique with higher time resolutions (up to 50 Hz) permits the obtaining of direct experimental information on grain growth kinetics during rapid heat treatment cycles that are of relevance for the HAZ. The present approach applies to bulk samples and, therefore, does not account for the steep spatial temperature gradients and associated potential thermal pinning that may occur in the HAZ. Meso-scale models, e.g. cellular automata or phase field models, are now available to consider these graded microstructures. These models need material-specific parameters that can be generated using the present approach.

Acknowledgement

References

[1] Guthrie RIL, Jonas JJ. ASM handbook: properties and selection: irons, steels and high performance alloys, 10th ed., vol. 1. Materials Park (OH): ASM International; 1990. p. 115–6.
[2] Militzer M, Giumelli AK, Hawbolt EB, Meadowcroft TR. Metall Mater Trans A 1996;27A:3399–409.
[3] Easterling K. Introduction to the physical metallurgy of welding. Oxford: Butterworth-Heinemann; 1992.
[4] Zhang LP, Davis CL, Strangwood M. Metall Mater Trans A 1999;30A:2089–96.
[5] Eroglu M, Aksoy M. Mater Sci Eng 2000;A286:289–97.
[6] Kou S. Welding metallurgy. 2nd ed. Hoboken, NJ: John Wiley & Sons; 2003.
[7] Ashby MF, Easterling KE. Acta Metall 1982;30:1969–78.
[8] Ion JC, Easterling KE, Ashby MF. Acta Metall 1984;32:1949–62.
[9] Gladman T. The physical metallurgy of microalloyed steels. London: The Institute of Materials; 2002.
[10] Manohar PA, Ferry M, Chandra T. ISIJ Int 1998;38:913–24.
[11] Bhadeshia HKDH, Honeycombe RWK. Steels microstructure and properties. Oxford: Elsevier; 2006.
[12] Gladman T, Pickering FB. Iron Steel Inst J 1967;205:653–64.
[13] Hunderi O, Ryum N. Acta Metall 1981;29:1737–45.
[14] Hillert M. Acta Metall 1988;36:3177–81.
[15] Andersen I, Grong Ø. Acta Metall Mater 1995;43:2673–88.
[16] Saito Y, Shiga C. ISIJ Int 1992;32:414–22.
[17] Senuma T, Suehiro M, Yada H. ISIJ Int 1992;32:423–32.
[18] Giumelli A, Militzer M, Hawbolt EB. ISIJ Int 1999;39:271–80.
[19] Danon A, Servant C, Almo A, Brachet JC. Mater Sci Eng A 2003;348A:122–32.
[20] Sahay SS, Malhotra CP, Kolkhede AM. Acta Mater 2003;51:339–46.
[21] San Marti D, Caballero FG, Capdevila C, Garcia de Andres C. Metall Mater Trans 2004;45:2797–804.
[22] Akselsen OM, Grong Ø, Ryum N, Christensen N. Acta Metall 1986;34:1807–15.
[23] Moon J, Lee J, Lee C. Mater Sci Eng A 2007;459:40–6.
[24] Mishra S, DebRoy T. Mater Sci Technol 2006;22:253–78.
[25] Lifshitz JM, Slyozov VV. J Phys Chem Solids 1961;19:35–50.
[26] Wagner C. Z Elektrochem 1961;65:581–91.
[27] Whelan MJ. Metal Sci J 1969;3:95–7.
[28] Ågren J. Scan J Metall 1990;19:2–8.
[29] Banerjee K, Militzer M, Perez M, Wang X. Metall Mater Trans A 2010;41A:3161–72.
[30] Hansen SS, Vander Sande JB, Cohen M. Metall Trans 1980;11A:387–402.
[31] Charleux M, Poole WJ, Militzer M, Deschamps A. Metall Mater Trans 2001;32A:1635–47.
[32] Dubois M, Moreau A, Militzer M, Bussière JF. Scripta Mater 1998;39:735–41.
[33] Dubois M, Militzer M, Moreau A, Bussière JF. Scripta Mater 2000;42:867–74.
[34] Krakauer BW, Moreau A. In: Brusey BW, Bussière JF, Dubois M, Moreau A, editors. International symposium on advanced sensors for metals processing. Montreal (Canada): MetSoc-CIM; 1999. p. 53–65.
[35] Kruger S, Moreau A, Lamouche G. In: Gottstein G, Molodov DA, editors. Proceedings of the 1st joint conference on 'recrystallization and grain growth'. Berlin: Springer; 2001. p. 583.
[36] Moreau A, Lévesque D, Lord M, Dubois M, Monchalin JP, Padioleau C, et al. Ultrasonics 2002;40:1047–56.
[37] Sarkar S, Moreau A, Militzer M, Poole WJ. Metall Mater Trans 2008;39A:897–907.
[38] Militzer M, Maalekian M, Moreau A. Proceedings of 'recrystallization and grain growth IV' (2010), Sheffield, UK, in press.
[39] Kruger S, Lamouche G, Monchalin JP, Kolarik II R, Jeskey G, Choquet M. AISTech Proc 2005;II:553–60.
[40] Militzer M, Hawbolt EB, Meadowcroft TR. Metall Mater Trans 2000;31A:1247–59.

[41] Sarkar S, Militzer M, Poole WJ, Moreau A. In: Szpunar JA, Li H, editors. Advanced steels. Montreal (Canada): MetSoc-CIM; 2006. p. 119–30.

[42] Baker RG, Nutting J. Precipitation processes in steels. London: The Iron and Steel Institute; 1959. p. 1–21.

[43] Patterson BR, Liu Y. Metall Trans 1992;23A:2481–2.

[44] Hellman P, Hillert M. Scand J Metall 1975;4:211–9.

[45] Humphreys FJ, Hatherly M. Recrystallization and related annealing phenomena. 2nd ed. Oxford: Elsevier; 2004.

[46] Hillert M. Acta Metall 1964;13:227–38.

[47] Zener C. Trans AIME 1948;175:15–51.

[48] Rios PR. Acta Metall 1987;35:2805–14.

[49] Uhm S, Moon J, Lee C, Yoon Y, Lee B. ISIJ Int 2004;44:1230–7.

[50] Janssens KGF, Raabe D, Kozeschnik E, Miodownik MA, Nestler B. Computational materials engineering: an introduction to microstructure evolution. Oxford: Elsevier; 2007.

[51] Svoboda J, Fischer FD, Fratzl P, Kozeschnik E. Mater Sci Eng A 2004;A385:157–65.

[52] Kozeschnik E, Svoboda J, Fratzl P, Fischer FD. Mater Sci Eng A 2004;A385:166–74.

[53] Kozeschnik E, Svoboda J, Fischer FD. CALPHAD 2004;28:379–82.

[54] Sonderegger B, Kozeschnik E. Metall Mater Trans 2009;40A:499–510.

[55] Vienna University of Technology. Thermodynamic database 'mc_steel' (version 1.86), diffusion database 'mc_sample_fe' (version 1.03). Vienna (Austria): Institute of Materials Science and Technology.

[56] Russell K. Adv Colloid Interf Sci 1980;13:205–318.

[57] Kampmann R, Wagner R. Decomposition of alloys: the early stages. Oxford: Pergamon Press; 1984. p. 91–103.

[58] Fazeli F, Tafteh R, Militzer M, Poole WJ. The international symposium on the recent developments in plate steels. Warrendale (PA): AIST; 2011. p. 343–50.

[59] Fazeli F, Militzer M. J Iron Steel Res Int 2011;18(Suppl. 1–2):658–63.